Monochiral tubular graphite cones formed by radial layer-by-layer growth

G. Y. Zhang, X. D. Bai, and E. G. Wang*
Institute of Physics, Chinese Academy of Sciences, Beijing 100080, China

Y. Guo and Wanlin Guo
Institute of Nano Science, Nanjing University of Aeronautics and Astronautics, 210016, China
(Received 28 December 2004; published 28 March 2005)

Multiwalled carbon nanotubes in the form of tubular graphitic cones (TGC) are grown at high yield. Structure analysis reveals that chirality of the multiple walls in a TGC are nearly identical to each other and preferentially zigzag. The formation of such TGCs is explained by two separate processes along radial and axial directions, respectively. The root-based radial growth is via a layer-by-layer mode that controls the chirality of tubes. The axial growth extends the tubules with nearly identical chiral angles. Total energy calculations indicate that the inner tube with near zigzag chirality is favored to template the growth of monochiral multiwalled structures, in good agreement with experiments.

DOI: 10.1103/PhysRevB.71.113411 PACS number(s): 81.07.De, 61.46.+w, 68.55.Ac, 73.22.−f

Carbon nanotubes[1] (CNTs) have attracted intense interest because they are potential building blocks for nanoelectronics. It is well known that the chirality of CNTs is an important parameter to the physical properties of these materials.[2–7] However, the chirality of CNTs produced by any method appears random thus far. Even for an individual multiwalled CNT, the chiralities of all the layers tend to be different and random.[8,9]

In a recent work, we reported a type of multiwalled CNT structure called tubular graphite cones[10] (TGCs). TGCs are similar in structure to multiwalled CNTs, but exhibit cone-shaped structures due to varying lengths of the multiple layers. In this paper, we show that the chiralities of the multiple layers are nearly identical, achieving monochiral multiwalled CNTs. The growth mechanism of the TGC structures is studied, with an emphasis on determination and understanding of the chirality of the TGCs. Based on systematic high-resolution transmission electron microscopy (HRTEM) and electron diffraction (ED) studies, we confirmed that most of the TGCs show the same chirality of preferably the zigzag type. The formation process of the TGC structures can be explained as two separate processes proceeding along the axial and radial directions, respectively. The radial growth is driven by the interlayer interaction. A layer-by-layer formation model in the radial direction has been developed, which accounts for the development of identical chirality for all of the graphite sheets in a TGC. In this model, we demonstrate that the initial nucleation of the seed graphene tubule plays a key role in the control of certain chiralities. The axial growth extends the as-formed graphitic stacking sequence. Extensive total energy calculations were performed within this model. The theoretical results are in good agreement with the experimental observations.

Aligned TGCs were grown on iron tips using the microwave plasma-assisted chemical vapor deposition (MPCVD) method. The mixture of CH_4 and N_2 was used as the reactive gas. The actual temperature is about 870–900 °C for the iron tips measured by an infrared thermometer. During growth, plasma near the iron tips discharges due to their sharp geometric shapes there and leads to the formation of petal-like graphite. Just below the discharged area, the TGCs grow out.[10] All TGCs have a length of tens of nanometers exhibit-faceted and cone-shaped surfaces. The tips of the TGCs are of nanometer scale, and the roots are of nanometer or micrometer scale, which can be controlled by the growth time. The Raman spectra of an isolated TGC indicate the high crystal quality.[11] The microstructure of the TGCs was found to be similar to that of CNTs in terms of their cylindrical graphite sheets and hollow nanometer-scale interiors. In contrast with the CNTs' structure, in which the graphite sheets are all equal in length, the cylindrical sheets of a TGC are gradually shorter, from inner to outer, and they terminate along the TGC's surface, forming a conical surface [see Fig. 1(a)]. The cone tips, which are made of several layers of graphite sheets, are usually not as perfectly crystallized as those of CNTs.

The obtained TGCs were characterized by HRTEM and ED. In this study, the incident electron beam direction for both cases is nearly normal to the cone axis. An ED pattern from individual TGC contains at least three types of reflexions: a row of $00l$ (l=even) reflexions, graphitelike $hk0$ reflexions, and $h0l$ (l=odd) reflexions (see Figs. 1 and 2). The $00l$ diffraction spots are distributed along the normal direction to the cone axis and sharply defined, while the $hk0$ diffraction spots are located at the vertices of hexagons inscribed in circles with radii g_{hk0} and streaked along the same direction in the sense away from the axis. This streaking phenomenon is attributed to the progressive narrowing, in that direction, of the apparent lattice spacing. The $hk0$ diffraction spots are believed to be associated with the "front" and "back" halves of cylindrical graphite sheets within a TGC in the tangent planes, perpendicular to the beam direction. The appearance of $h0l$ diffraction spots in the diffraction pattern is obviously an artifact of the graphitic stacking of wall layers. The front and back hemicylindrical parts of a graphite sheet project on the plane perpendicular to the beam direction in two networks, which are rotated from each other by twice of the chiral angle θ. As a consequence, the diffraction patterns produced by them are rotated by the same angle 2θ, so that the chiral angles of the graphite sheets can be obtained by measuring the half of the angular separations between these pairs of first-order hexagons.[12–15]

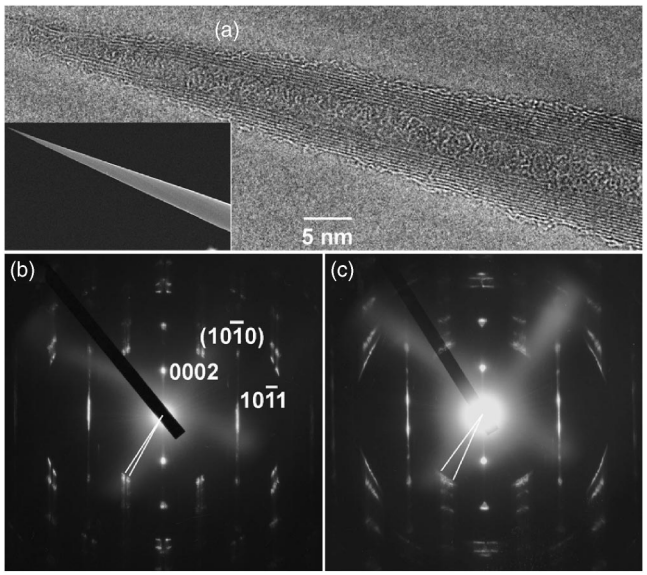

FIG. 1. (a) The HRTEM image of a TGC tip. The diameter of its hollow interior is about 2 nm and the graphite layer steps on its surface can be easily seen. The inset shows the scanning electron micoscope image of a typical TGC. (b) and (c) are the ED patterns taken from two different individual TGCs. (b) shows that the overall graphite sheets of a TGC have roughly the same chiralities with a chiral angle of about 2.2°, and (c) shows that the chiral angles of overall graphite sheets of another TGC are in the region of 0° to 6°.

The chirality of the TGCs was studied over a large number of samples based on their ED patterns. For most samples, only few (usually one or two) specific kinds of chiralities are observed from individual cones even if they consist of over hundreds of wall layers [Fig. 1(b)]. A fraction of samples with other chiralities [Fig. 1(c)] were also observed, but they are rare. Most interestingly, we found that the chiral angle of all graphite sheets in the obtained TGCs is close to 0° and most of them have an identical zigzag chirality, i.e., the chiral angle of 0°, for their inner graphite sheets. Figures 2(b)–2(d) show an example of the typical ED patterns of a single cone taken from different regions from tip to root, which unambiguously show the identical zigzag chirality. These patterns exhibit essentially the same features despite the different density of diffraction spots, and reveal that the identical zigzag chirality feature is not a local phenomenon. The measured average interlayer spacing d_{002} from the ED patterns is 0.335–0.338 nm. The constant $d_{100}=0.213$ nm was used as a calibration standard, based on the fact that the C-C bond lengths are the same for both this tubular structure and bulk graphite.[16]

The HRTEM lattice image of the cones with zigzag-type monochirality exhibits some unusual features compared to that of the multiwalled CNTs. First, two-dimensional lattice fringes can be clearly resolved in the cone wall area [Fig. 2(e)]. The fringes parallel to the cone axis are obviously the graphite (0002) lattice fringes, while the 0.2 nm lattice fringes can be assigned to the (10$\bar{1}$1) lattice fringes indicated by the fast Fourier transforms (FFTs) of the HRTEM image [inset of Fig. 2(e)]. Second, the hexagonal pattern appears in the cone's central region at the same time [Fig. 2(f)]. This

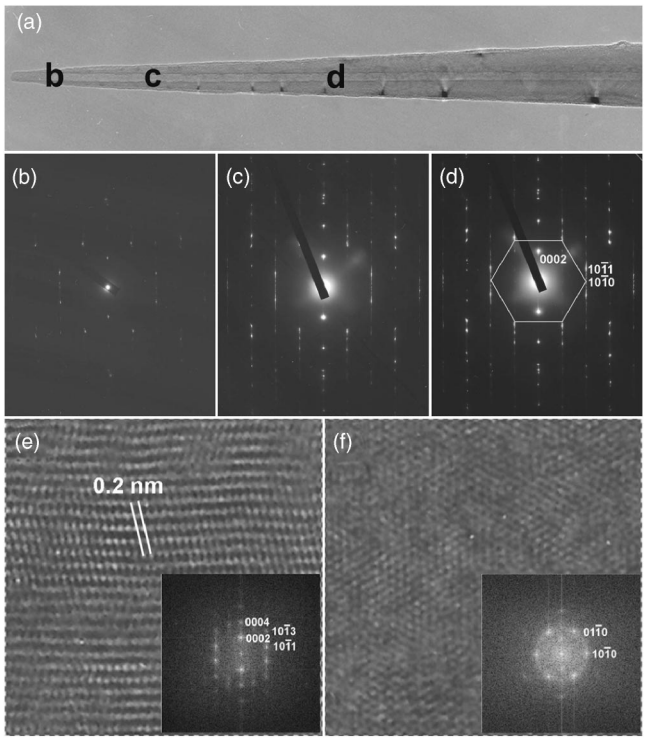

FIG. 2. The ED and HRTEM results of a TGC with identical zigzag chirality. (a) shows a low magnification TEM image of the TGC; (b), (c), and (d) are three ED patterns taken from different regions from its tip to root [marked by (b), (c), and (d), respectively in (a)]; (e) and (f) are HRTEM lattice fringe images recorded from the wall and the center areas of the TGC, and their corresponding FFT images are shown in the insets of (e) and (f), respectively.

pattern also overlaps some of the innermost wall layers, especially when the diameter of the outer layers is large. The FFTs in Fig. 2(f) show that the hexagonal patterns originate from the reflexions of {10$\bar{1}$0} planes. The overlapping of the two FFT images is in good agreement with the ED patterns shown in Fig. 2(b)–2(d).

It is interesting to note that all TGCs keep their cone-shaped structure with nearly the same apex angle no matter where the growth is terminated. Thus the TGC growth can be reasonably decomposed into axial and radial directions, respectively, as the schematic in Fig. 3. Although the axial and radial growth process has been discussed previously for vapor-grown carbon nanofibers (ie., in Ref. 17), here we present a different growth process and resulting CNT structure. The root-based radial growth is a process of continuous nucleation of new tubular layers outside the inner layers. A layer-by-layer growth model can describe this continuous formation of additional tubular sheets along the radial direction. In this model, the interaction between neighboring layers is important, with the result that all of the graphite layers of a single cone have a monochirality, i.e., the seed tube's chirality. Simultaneously, the axial growth elongates the formed tubular graphite sheets along the axial direction and keeps the as-formed sticking sequence. It was found that the iron substrate plays an important role in the axial growth as nothing was observed when we changed to a tungsten tip covered by thin iron layers under the same conditions.[9] The

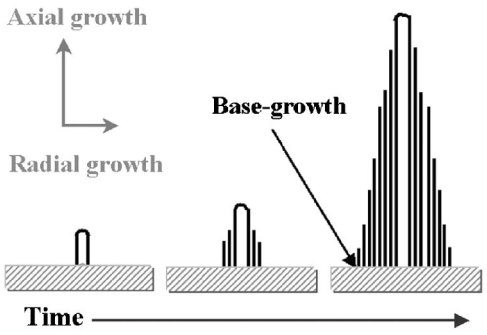

FIG. 3. A schematic of the formation process for a TGC structure. The axial growth elongates the as-formed graphite sheet lengths, while the root-based layer-by-layer radial growth increases the tube thickness.

conical shape of the TGCs was controlled by the axial growth rate (R_a) and the radial growth rate (R_r). Here R_a is much larger than R_r. The tip size of the TGCs varies from several nanometers to tens of nanometers. This indicates that the initial nucleation may be assisted by a dynamic formation and restructuring of monoatomic step edges at the catalyst surface.[18]

The total energy of the TGC structures has been calculated by using a molecular statics method[19,20] to understand the experimental observations of the nearly identical chirality. For simplicity, a double-walled tube is considered as a model, and the inner tube acts as a seed. For a (n,m) tube $(n \geqslant m)$,[21] its radius is given by $R=(\sqrt{3}a_{c-c}/2\pi)\sqrt{n^2+m^2+nm}$, where a_{c-c} (1.42 Å) is the length of the C—C bond. For a given seed tube, there are many possible outer tubes with different indexes of (n,m). According to the experimental results, we set the outer tubes' radius to satisfy the condition $R_{seed}+3.23\ \text{Å} \leqslant R_{outer} \leqslant R_{seed}+3.53\ \text{Å}$. The chirality-dependent K—C potential[20] is used to describe the interlayer interaction. Four zigzag (26,0), (50,0), (100,0), and (200,0) tubes with radii of 10.2, 19.6, 39.1, and 78.3 Å are selected as the seed tubes for examples. To simulate the layer-by-layer growth, the total energies of all possible tubular configurations forming on the outside of the three seeds are calculated. Figure 4(a) shows the variations of the minimum interlayer potential energy for the different outer tubes when m/n ranges from 0 to 1. It is interesting to note that the interlayer energies are always lowest when both outer and inner tubes are zigzag type $(m/n=0)$. The energy gaps (in kcal/mol/atom) between the lowest minimum interlayer energy and the next one are larger than 0.03423 for all samples. The significant energy difference indicates that the outer tubular graphite sheets prefer to have the same chirality when the inner tube is a zigzag tube. However, it does not happen when the seed tubes have a large chiral angle, for example of armchair type, based on our calculations. These results reveal that the identical chiralities are preferred if the seed tubes have small chiral angles and the interlayer interaction is the main driving force in radial growth.

Furthermore, we have studied the diameter effects for zigzag-type seed tubes from (26,0) to (400,0) with radii in the range of 1–16 nm. The minimum interaction energy decreases drastically with the increase of the tube radius [see Fig. 4(b)]. A sharp decrease of the intertube energy occurs in the region of smaller tubes. When the seed tube radius goes larger, for example larger than 10 nm, the interlayer interaction energy of the system approaches a constant.

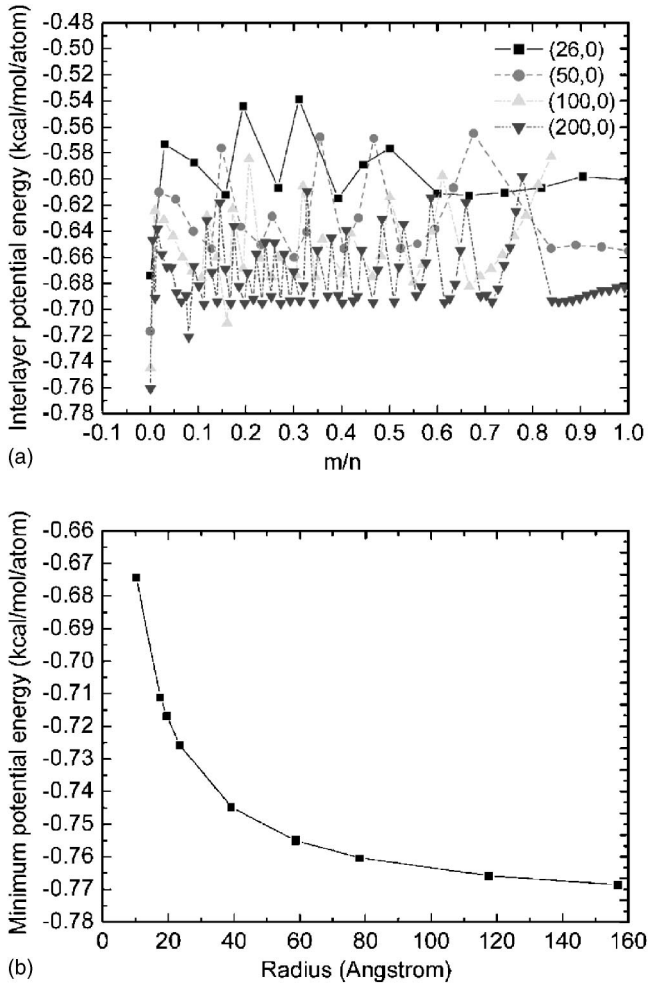

FIG. 4. (a) For different seed tubes of (26, 0), (50, 0), (100, 0) and (200, 0), the minimum interlayer interaction energy varies with n/m, where integers n and m denote the orientation of the outer tubes. (b) The minimum interlayer interaction energy of a zigzag outer tube varies with the radius of a zigzag seed tube.

In conclusion, multiwalled carbon nanotube cones are grown at high yield and the chiralities of the multiple walls in a cone are nearly identical to each other and preferentially zigzag. Monochiral multiwalled nanotubes are synthesized. It was found that the formation of the cone structure is controlled by radial and axial growth. Root-based radial growth determines the chirality, while axial growth extends the ordered stacking of graphite sheets. A layer-by-layer growth model has been proposed in the radial direction, which reveals why all graphite sheets in a TGC have nearly identical chirality when the seed tubes have small chiral angles. We show that the initial nucleation of the seed graphene tube is very important in controlling certain chiralities. The good agreement between theory and experiment suggests that the present model and understanding could be useful in the practice of controlling chirality in the synthesis of CNTs.

The authors thank Hongjie Dai, Lu-Chang Qin, Zhong L. Wang, and Xin Jiang for many helpful discussions and acknowledge financial support from NSF (Grant Nos. 60021403, 10134030, 10540420033), MOST (Grant Nos. G2000067100, 2002AA311150), and CAS of China.

*Author to whom correspondence should be addressed. Electronic address: egwang@aphy.iphy.ac.cn

[1] S. Iijima, Nature (London) **354**, 56 (1991).
[2] N. Hamada, S. Sawada, and A. Oshiyama, Phys. Rev. Lett. **68**, 1579 (1992).
[3] R. Saito, M. Fujita, G. Dresselhaus, and M. S. Dresselhaus, Appl. Phys. Lett. **60**, 2204 (1992).
[4] Y. Yaish, J. Y. Park, S. Rosenblatt, V. Sazonova, M. Brink, and P. L. McEuen, Phys. Rev. Lett. **92**, 046401 (2004).
[5] A. N. Kolmogorov, V. H. Crespi, M. H. Schleier-Smith, and J. C. Ellenbogen, Phys. Rev. Lett. **92**, 085503 (2004).
[6] P. G. Collins, M. S. Arnold, and P. Avouris, Science **292**, 706 (2001).
[7] R. Krupke, F. Hennrich, H. v. Lohneysen, and M. M. Kappes, Science **301**, 344 (2003).
[8] M. Ge and K. Sattler, Science **260**, 515 (1993).
[9] M. Liu and J. M. Cowley, Carbon **32**, 393 (1994).
[10] G. Y. Zhang, X. Jiang, and E. G. Wang, Science **300**, 472 (2003).
[11] G. Y. Zhang, X. D. Bai, X. Jiang, and E. G. Wang (unpublished).
[12] X. F. Zhang, X. B. Zhang, G. Van Tendeloo, S. Amelinckx, M. Op de Beeck, and J. Van Landuyt, J. Cryst. Growth **130**, 368 (1993); X. B. Zhang, X. F. Zhang, S. Amelinckx, G. Van Tendeloo, and J. Van Landuyt, Ultramicroscopy **54**, 237 (1994).
[13] S. Iijima and T. Ichihashi, Nature (London) **363**, 603 (1993).
[14] L. C. Qin, T. Ichihashi, and S. Iijima, Ultramicroscopy **67**, 181 (1997).
[15] Ph. Lambin, V. Meunier, L. Henrard, and A. A. Lucas, Carbon **38**, 1713 (2000).
[16] Y. Saito, T. Yoshikawa, S. Bandow, M. Tomita, and T. Hayashi, Phys. Rev. B **48**, 1907 (1993).
[17] T. Koyama and M. Endo, Oyo Butsuri **42**, 690 (1973).
[18] S. Helveg, C. López-Cartes, J. Sehested, P. L. Hansen, B. S. Clausen, J. R. Rostrup-Nielsen, F. Abild-Pedersen, and J. K. Nørskov, Nature (London) **427**, 426 (2004).
[19] A. N. Kolmogorov, V. H. Crespi, M. H. Schleier-Smith, and J. C. Ellenbogen, Phys. Rev. Lett. **92**, 085503 (2004).
[20] A. N. Kolmogorov and V. H. Crespi, Phys. Rev. Lett. **85**, 4727 (2000).
[21] N. Hamada, S. Sawada, and A. Oshiyama, Phys. Rev. Lett. **68**, 1579 (1992).